Long-Term Reliability Degradation of Ultrathin Dielectric Films Due to Heavy-Ion Irradiation

B. K. Choi, *Member, IEEE*, D. M. Fleetwood, *Fellow, IEEE*, R. D. Schrimpf, *Fellow, IEEE*, Lloyd W. Massengill, *Senior Member, IEEE*, K. F. Galloway, *Fellow, IEEE*, M. R. Shaneyfelt, *Fellow, IEEE*, T. L. Meisenheimer, *Member, IEEE*, P. E. Dodd, *Member, IEEE*, J. R. Schwank, *Fellow, IEEE*, Y. M. Lee, R. S. John, and G. Lucovsky, *Member, IEEE*

***Abstract*—High-energy ion-irradiated 3.3-nm oxynitride film and 2.2-nm SiO_2-film MOS capacitors show premature breakdown during subsequent electrical stress. This degradation in breakdown increases with increasing ion linear energy transfer (LET), increasing ion fluence, and decreasing oxide thickness. The reliability degradation due to high-energy ion-induced latent defects is explained by a simple percolation model of conduction through SiO_2 layers with irradiation and/or electrical stress-induced defects. Monitoring the gate-leakage current reveals the presence of latent defects in the dielectric films. These results may be significant to future single-event effects and single-event gate rupture tests for MOS devices and ICs with ultrathin gate oxides.**

***Index Terms*—Heavy-ion irradiation, radiation effect, single-event effect, ultra-thin gate dielectric films.**

I. Introduction

As MOS devices continue to scale down in dimension and gate oxides become increasingly thinner, more and more attention is being paid to reliability concerns associated with ultrathin dielectrics. While single-event gate rupture (SEGR) due to heavy ion exposure for MOS devices has received considerable attention in space and avionics applications [1], [2], the post-ion-exposure reliability of devices with thin gate oxides has received far less attention. Recently, Suehle *et al.* reported latent reliability degradation of 3.0-nm SiO_2 films after high-linear energy transfer (LET) irradiation [3]. In addition, the degradation of 3.3-nm oxynitride films due to heavy-ion irradiation has been reported [4].

Based on the previous experimental results and new ones we show in this paper on fluence, ion LET, and oxide thickness dependence, we propose here a model based on a percolation approach [5] to explain the mechanism of the reliability degradation of dielectric films due to high-energy ion irradiation. A method of examining ion-induced defect generation by monitoring the gate leakage current also is described. The implications are discussed for space applications and heavy-ion testing of microelectronics with thin gate dielectrics.

Manuscript received July 15, 2002; revised September 20, 2002. This work was supported in part by the U.S. Air Force Office of Scientific Research through a Multidisciplinary University Research Initiative (MURI), and by the Defense Threat Reduction Agency under Contract DTRA01-00-C-0010. Sandia is a multiprogram laboratory operated by Sandia Corporation, a Lockheed-Martin Company, for the United States Department of Energy, under Contract DE-AC04-94AL85000.

B. K. Choi, D. M. Fleetwood, R. D. Schrimpf, L. W. Massengill, and K. F. Galloway are with the Department of Electrical Engineering and Computer Science, Vanderbilt University, Nashville, TN 37235 USA (e-mail: bo.choi@vanderbilt.edu; bo.k.choi@ieee.org).

M. R. Shaneyfelt, T. L. Meisenheimer, P. E. Dodd, and J. R. Schwank are with Sandia National Laboratories, Albuquerque, NM 87135 USA.

Y. M. Lee is with the Department of Electrical and Computer Engineering, North Carolina State University, Raleigh, NC 27607 USA.

R. S. John and G. Lucovsky are with the Department of Physics, North Carolina State University, Raleigh, NC 27607 USA.

Digital Object Identifier 10.1109/TNS.2002.805389

II. Samples and Experiments

Three types of capacitors, all on p-type silicon substrates, were studied: 3.3-nm (physical thickness) plasma enhanced chemical vapor deposition (PECVD) oxynitride films with polysilicon gate electrodes; 3.3-nm PECVD SiO_2 films with polysilicon gate electrodes; and 2.2-nm PECVD SiO_2 films with Al gate electrodes [2], [6]. Two different capacitor sizes were used for this study: $100 \times 100\ \mu m^2$ and $50 \times 50\ \mu m^2$. The device area is isolated by 200-nm field oxide, and the active area was defined by wet-etching of the field-oxide layer.

Heavy-ion irradiation was performed at the Brookhaven National Laboratory Tandem Van de Graaff facility using 342-MeV Au (LET = 82.0 MeV/mg/cm^2), 339-MeV I (LET= 59.8 MeV/mg/cm^2), and 285-MeV Br (LET = 37.2 MeV/mg/cm^2) ions. The irradiated capacitors were subjected to a voltage step-stress test with 0.1-V steps and 10 s duration for each step. The quantity of injected charge was obtained by numerical integration of the measured gate current.

Fig. 1 illustrates the breakdown-measurement sequence. During the voltage step-stress test, the gate-leakage current is measured using an HP4155 semiconductor parameter analyzer. Between each voltage step, a voltage sweep is performed and the current is measured to monitor the variation of the gate current versus voltage characteristics. The voltage step-stress procedure has been used for SEGR experiments [2], [4], [7]. During the SEGR experiments, the time period of each voltage step was dependent on the flux of the ion beam and a target fluence. In Fig. 1, the postirradiation stress curves exhibit early breakdown and larger leakage currents at moderate stress voltages.

III. Results and Observations

Three major parameters have been observed to affect postirradiation reliability degradation [3], [4]: film thickness, ion LET, and ion fluence. Premature breakdown during postirradiation electrical stress has been observed in 3.3-nm oxynitride and SiO_2 films and 2.2-nm SiO_2 films. Seuhle *et al.* [3] reported

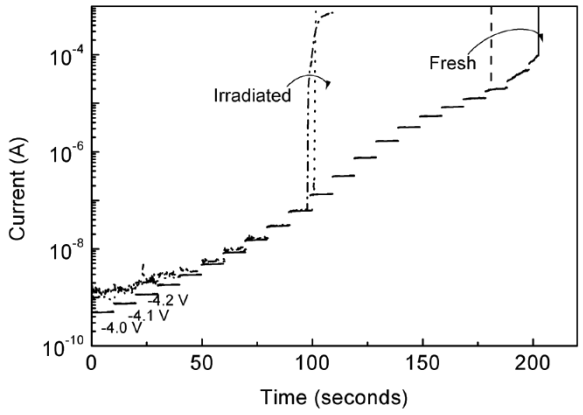

Fig. 1. A measurement procedure of injected charge and breakdown. During a voltage applied by 0.1-V steps for 10 s, a gate current is monitored and integrated until breakdown. An amount larger than 100× the gate current increase during a voltage stress step is determined as breakdown. Two samples of unirradiated and irradiated capacitors are shown in this figure.

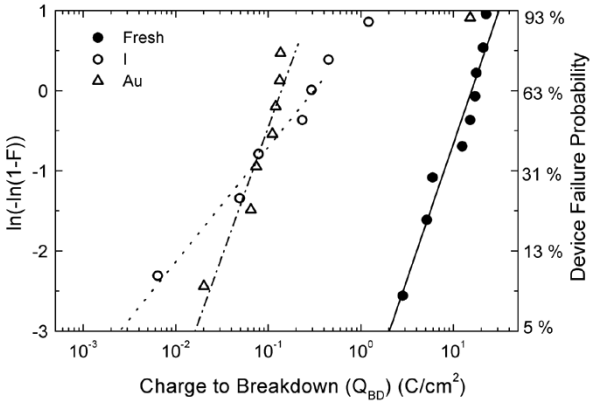

Fig. 2. Charge to breakdown (Q_{BD}) for 3.3-nm oxynitride film MOS capacitors. F is device failure probability. This plot shows Weibull distributions. The area of all the capacitors is 50 × 50 μm^2 and the gate electrodes were floating during irradiation. (a) (•) before irradiation ($Q_{BD} = 15.7$, $W_E = -4.039 + 1.467\ln(Q)$, median $V_{BD} = -6.0$ V); (b) (∘) after 339 MeV I 4.0 × 10^7 ions/cm^2 fluence ($Q_{BD} = 0.3$, $W_R = 0.717 + 0.618\ln(Q)$, median $V_{BD} = -5.2$ V); and (c) (△) after 342 MeV Au 1.8 × 10^7 ions/cm^2 fluence ($Q_{BD} = 0.1$, $W_R = 2.814 + 1.406\ln(Q)$, median $V_{BD} = -4.7$ V).

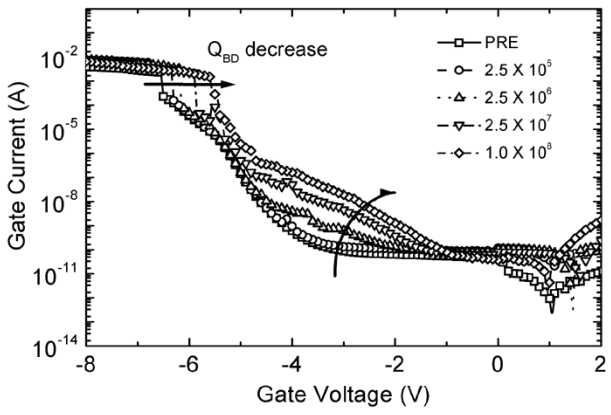

Fig. 3. Gate current versus gate voltage after 342 MeV Au ion irradiation at various fluences. The area of all the capacitors is 100 × 100 μm^2 and the gate electrodes were grounded during irradiation. The capacitors consist of 3.3-nm oxynitride film and the unit of each fluence is ions/cm^2. The leakage current change near −2.5 V is clear with increasing fluence and the charge to breakdown decrease in the FN tunneling dominant regime is also obvious.

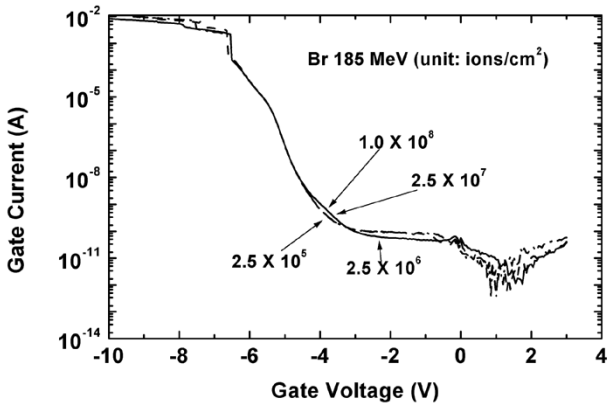

Fig. 4. Gate current versus gate voltage after Br 185-MeV ion irradiation at various fluences. The area of all the capacitors is 100 × 100 μm^2 and the gate electrodes were grounded during irradiation. The capacitors consist of 3.3-nm oxynitride film and the unit of each fluence is ions/cm^2.

the same kind of degradation on 3.0-nm SiO_2 films. For thicker films, Sexton *et al.* [7] reported little degradation on 7.0-nm SiO_2 films and Choi *et al.* [4] showed the robustness of 5.6-nm Al_2O_3 films after 342-MeV Au ion irradiation. These results indicate that premature breakdown due to ion irradiation is a much more significant concern for ultrathin oxides than for thicker oxides and/or alternative dielectrics with greater physical thicknesses than the thinner SiO_2 layers they are intended to replace.

Fig. 2 is a statistical summary of measured breakdown phenomena for several capacitors. This Weibull plot shows that the charge to breakdown is degraded by two orders of magnitude for capacitors irradiated with either 342-MeV Au or 339-MeV I ions at a fluence level of 10^7 cm^{-2}. During the irradiation in Fig. 2, the gate electrodes of the capacitors were floating and substrates were grounded. Results with grounded gate electrodes are shown in Fig. 3, which is a plot of gate current versus gate voltage for different Au-ion fluences; the degradation behavior is similar to the floating gate case.

As shown in Fig. 3, the reliability of ultrathin oxide films has started to be degraded at a fluence level of the order of 10^6/cm^2 for 342 MeV Au ions. In the case of intermediate LET 285 MeV Br ions, neither the gate-leakage current nor the breakdown behavior shows a significant change up to 10^8/cm^2 fluence (Fig. 4). This behavior of the gate leakage current due to heavy-ion irradiation is consistent with the results on 7-nm thickness oxide films obtained by Sexton *et al.*, which showed very little enhanced current leakage after similar fluences of Br ion exposure [7]. In addition, Suehle *et al.* [3] found that gamma-ray irradiation has little effect on 3.0-nm SiO_2 films up to 300 kGy dose.

Fig. 5 shows the enhancement of the reliability degradation due to increasing incident ion fluence. This result is for 2.2-nm SiO_2 films with 342-MeV Au ions. Suehle *et al.* showed the same trends on 3.0-nm SiO_2 films with 823-MeV Xe ions (LET = 59 MeV/mg/cm^2) [3]. In Figs. 2 and 5, the voltage to breakdown should be taken into account with the measured charge to breakdown to compare the results from the constant voltage stress method, e.g., in [3].

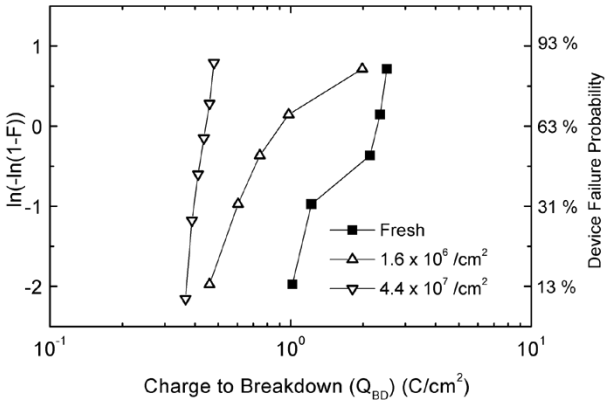

Fig. 5. Fluence dependence of postirradiation reliability degradation for 2.2-nm SiO_2 films. The incident ion was 342 MeV Au. The size of capacitors is $50 \times 50\ \mu m^2$. The median breakdown voltage is -4.5 V for the unirradiated set, -4.1 V for 1.6×10^6 ions/cm^2, and -3.7 V for 4.4×10^7 ions/cm^2, respectively.

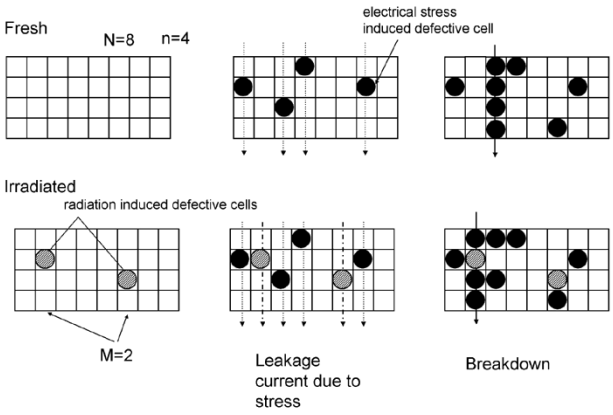

Fig. 6. Schematic picture showing the generation of defective cells and the breakdown condition due to electrical stress in fresh and high-LET ion-irradiated films: N is the total number of columns, n is the number of cells in a column, and M is the total number of columns that contain radiation-induced defective cells.

The fact that at least at fluences of interest to most space systems [2], this effect is primarily observed only for very high-LET ion at fluences above 10^6 ions/cm^2 means that this may not be a significant reliability concern in space operation for systems with these kinds of devices. However, it is quite possible that this effect may complicate the interpretation of heavy-ion test data for high-LET ions, as it makes it more likely that one will see dielectric breakdown during a single-event upset test, for example.

IV. A Statistical Model

We now describe a model to explain why reliability can degrade by ion irradiation. A schematic picture of this model is shown in Fig. 6, which is based on Suñé's simple percolation approach [5]. Electrical stress is envisioned to produce defective cells in the percolation breakdown model [8]. These cells contribute to the stress-induced leakage current (SILC) of MOS capacitors [9]. As the spacing between defective cells becomes smaller, dielectric film breakdown occurs as complete current paths are formed between the gate and substrate electrodes. If high-LET ions produce defective cells that act as latent current paths, the amount of subsequent electrical stress required to trigger breakdown is less than in the unirradiated case. In contrast, the formation of latent defect paths is apparently less efficient for lower-LET ion irradiation.

TABLE I
Summary of Mathematical Descriptions of the Model of Fig. 6

Description	Fresh device	Irradiated device
Cell cumulative failure probability (F_{cell})	λ_E	λ_R or λ_E
Column cumulative failure probability (F_{col})	λ_E^n	$\lambda_R^m \lambda_E^{n-m}$
Device cumulative reliability $(1-F)$	$(1-\lambda_E^n)^N$	$(1-\lambda_E^n)^N \times (\frac{1-\lambda_R^m \lambda_E^{n-m}}{1-\lambda_E^n})^M$
Weibull distribution $\ln[-\ln(1-F)]$	$W_E = \ln[N\lambda_E^n]$	$W_{R+E} = \ln[N\lambda_E^n + M(\frac{\lambda_R^m \lambda_E^{n-m} - \lambda_E^n}{1-\lambda_E^n})]$

A mathematical description of the high-LET damage model is presented in Table I. The expressions for unirradiated devices were introduced by Suñé [5]. We assume that the defective cells caused by high-LET ion stress have a different probability for failure independent of subsequent electrical stress, and the number of defective cells per defective column is identical in the whole film. Even if each ion-induced defective cell has different failure probability, the device failure occurs by the weakest links in the whole film. Hence, we think this simplification can help the interpretation of this degradation mechanism.

Suñé's model is an extended and discretized one-dimensional problem of $N \times n$ cells: N is the total number of columns and n is the number of cells in a column. Hence, the thickness of films can be represented in terms of n, and N is proportional to the area of the device. The failure probability of each cell is given by λ. The cell failure probability is known to be enhanced by electrical stress. To differentiate the source of degradation, we introduce a subscript E for electrical stress and R for radiation stress in Table I. Assuming $M \times m$ cells out of $N \times n$ total number of cells became defective after high-LET ion irradiation: M is the total number of columns that contain radiation induced defective cells; m is the number of defective cells per column. These defective cells have different failure probability as described earlier. Hence, the cells are divided into two kinds: $M \times m$ cells of failure probability λ_R, which is independent of subsequent electrical stress; and $N \times n - M \times m$ cells of failure probability λ_E, which is enhanced by electrical stress. It is reasonable that m is assumed to be less than n, otherwise the column is already a conductive path. The mathematical procedures used to solve the model equations in Table I are described in [5].

In the case of thicker films with the same amount of defective cells as in ultrathin films, i.e., a certain m and M, the device cumulative reliability ($1-F$ in Table I) is almost the same in either irradiated or fresh devices: for $n \gg m$, and $N > M$

$$1-F=(1-\lambda_E^n)^N\left(\frac{1-\lambda_E^{n-m}\lambda_R^m}{1-\lambda_E^n}\right)^M \approx (1-\lambda_E^n)^N. \quad (1)$$

Equation (1) illustrates why 7-nm SiO_2 films [7] and 5.6-nm Al_2O_3 films [4] did not suffer measurable reliability degradation even after irradiation with high-LET ions up to a fluence of 10^8 cm^{-2}.

On the other hand, this model shows that the Weibull distribution of breakdown statistics of high-LET ion irradiated ultrathin films (W_{R+E}) has a larger value than that in unirradiated films (W_E): from Table I, subtracting W_E from W_{R+E} yields

$$W_{R+E}-W_E=\ln\left[1+\frac{M}{N}\frac{(\lambda_R/\lambda_E)^m-1}{1-\lambda_E^n}\right]. \quad (2)$$

The right side of this equation is greater than 0, for $\lambda_R > \lambda_E$. This equation indicates postirradiation reliability degradation. It is reasonable to consider that the reliability changes only for the regime in which the probability of cell failure in unirradiated devices is low. Thus, the assumption that $\lambda_R > \lambda_E$ is valid for this discussion. Equation (2) also shows that the change of the Weibull distribution due to high-LET ion irradiation will be larger for thinner films, i.e., smaller n. Meanwhile, the number of columns (M) that contain radiation-induced defects is proportional to fluence times defect generation yield. Thus, the Weibull distribution of breakdown statistics of high-LET ion-irradiated capacitors is a function of the fluence.

We now introduce an extreme case example in order to show how this model works qualitatively. Let us assume that the cell failure probability of defect cells is 1.0, which is equivalent to a complete conducting path, and each defective column has a single defective cell, i.e., $m = 1$. According to the model in Table I, this extreme case is mathematically identical with a partial thinning effect of the dielectric film. Fig. 7 shows the change in the Weibull distribution of a degraded film with $N = 10^7$ and $n = 3$. For the same conditions with thicker films, i.e., $n > 3$, there will be less change in the Weibull distribution with the same amount of damaged area. This calculation illustrates that the model explains the dependence of postirradiation reliability degradation on film thickness and ion fluence.

We now consider the effect of ion LET on the degradation mechanism. An extremely large amount of local energy deposition is necessary to generate the kinds of defect clusters that are required to generate the defective regions pictured in Fig. 6. Hence, it is reasonable that high-LET ions can more easily cause enhanced leakage current and/or premature oxide breakdown than lower-LET ions. The higher the LET of the ion, by definition, the greater is the energy deposited per unit path length, and the more likely it is that one can generate a defect cluster in the dielectric layer. We will discuss the defect generation yield using the gate leakage current in the following section.

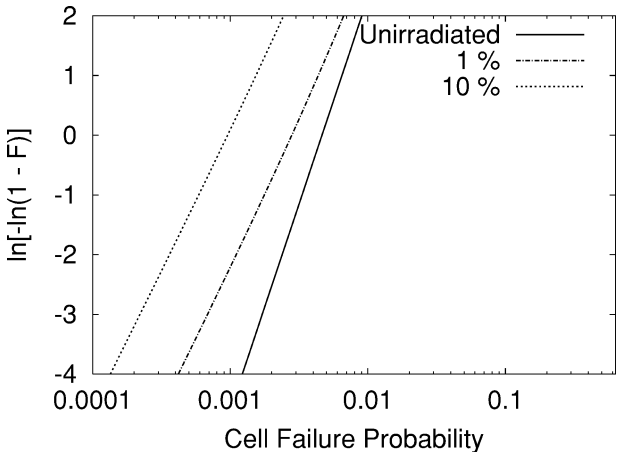

Fig. 7. Calculated Weibull distribution change by defects due to high-LET ion irradiation. The percent damage represents the defective area ratio. Here we assume that $n = 3$, $m = 1$, $N = 10^7$, and $M = 10^6$ (10%), 10^5 (1%). For this extreme case calculation, each defective cell is assumed to have a failure probability of 1.0, i.e., $\lambda_R = 1.0$.

V. Latent Breakdown Paths and the Gate-Leakage Current

To verify that latent breakdown paths are produced by the defect clusters induced by high-LET ions, the quantum point contact (QPC) theory [9] was applied. Cester *et al.* have successfully applied QPC theory to study radiation-induced soft breakdown (RSB) and showed the existence of latent breakdown paths due to heavy-ion irradiation [10]. Our work uses the log-slope of the radiation-induced leakage current rather than RSB, because the fluence levels in which we are interested are far lower than those required to cause RSB in these devices.

According to QPC theory for SILC [9], the gate leakage current can be described in an analytical form as follows:

$$I_g=\frac{4q}{h\alpha}N\exp(-\alpha\psi-2Kt_{ox})\sinh\left(\frac{\alpha q}{2}(V_g-V_0)\right). \quad (3)$$

In the regime in which we are interested, i.e., $V_g \gg V_0$, we can simplify this equation as follows:

$$I_g \approx NJ_0\exp\left(\frac{\alpha q}{2}V_g\right).$$

Equation (3) represents the trap-assisted tunneling current; α is related to the transmission coefficient or tunneling probability of the point contacts; ψ is the energy level of the traps relative to the Fermi energy; t_{ox} is dielectric film thickness; K is an empirical constant; h is Planck's constant; q is the magnitude of electron charge; and N is the total number of current paths (related to the area of the device). If we take the logarithm of both sides, (3) can be rewritten in the form

$$\ln(I_g)=A+B\cdot V_g. \quad (4)$$

From (3), we see that the constants A and B of the earlier equation imply a semilinear relationship, i.e.,

$$A=-2\psi\cdot B-\ln(B)+C\approx -2\psi\cdot B+C. \quad (5)$$

Hence, the slope (B) of the log of the gate leakage current versus the gate voltage denotes the tunneling probability of a charge that is assisted by a trap in the dielectric film. From the relationship with the intercept (A) of the semi-log plot, i.e., $\ln(I_g)$ versus V_g, we can get information about the energy level of a

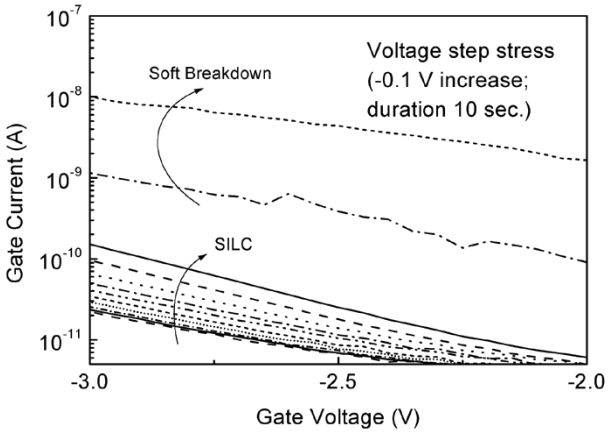

Fig. 8. Measured $\ln I_g$ versus V_g curves for an unirradiated 3.3-nm oxynitride film capacitor. Each curve was measured between each stressing voltage steps. The area of capacitor is $50 \times 50\ \mu\text{m}^2$.

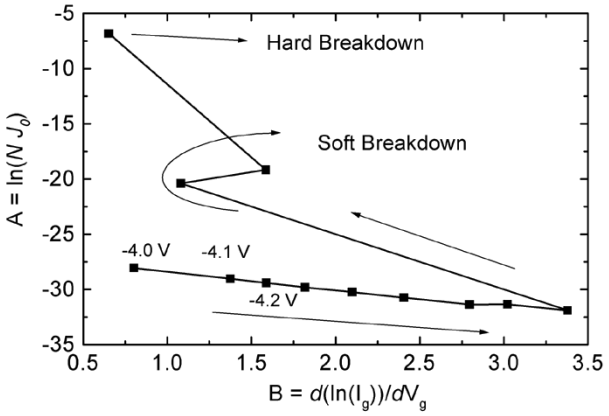

Fig. 9. Intercept (A) versus the slope (B) of the $\ln I_g$ versus V_g curve for an unirradiated 3.3-nm oxynitride film capacitor. Each data point was extracted from measured $\ln I_g$ versus V_g curves at $V_g = -2.5$ V in Fig. 8.

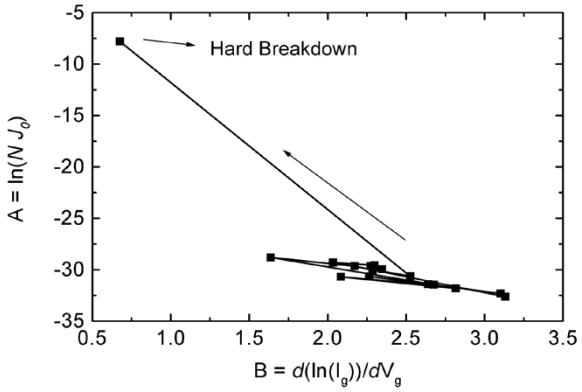

Fig. 10. Intercept (A) versus the slope (B) of the $\ln I_g$ versus V_g curve for an irradiated 3.3-nm oxynitride film capacitor: the incident ions are 342 MeV Au at 4.0×10^7 ions/cm^2 fluence. Each data point was measured at $V_g = -2.5$ V between each stressing voltage steps.

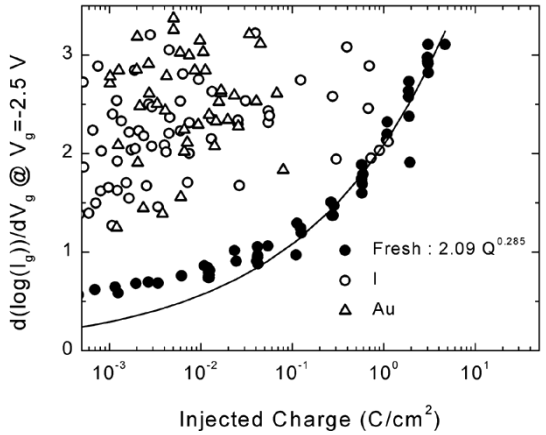

Fig. 11. Calculated log-slope of gate current ($d(\ln(I_g)/dV_g)$ at $V_g = -2.5$ V. The data were collected from current–voltage (I–V) curves between voltage stress steps. The area of all the capacitors is $50 \times 50\ \mu\text{m}^2$. The capacitors consist of 3.3-nm oxynitride film and the data were screened by goodness of fit to a linear curve. (a) (•) before irradiation ($Q_{BD} = 15.7$); (b) (○) after 339 MeV I 4.0×10^7 ions/cm^2 fluence (mean = 2.2); and (c) (△) after 342 Au MeV 1.8×10^7 ions/cm^2 fluence (mean = 2.6).

trap that contributes to the gate leakage current. The constant C consists of parameters related to physical dimensions and the number of current paths. A comparison of the Cs in the same structure and size devices can provide a ratio of the number of current paths.

Fig. 9 presents the intercept (A) versus the slope (B) extracted from measured $\ln I_g$ versus V_g curves (Fig. 8) for an unirradiated 3.3-nm oxynitride capacitor. Each data point was measured at $V_g = -2.5$ V between each stressing voltage step. For unirradiated films, the slope (B) increases with electrical stress in the SILC regime, and after a certain threshold of electrical stress, the device shows soft breakdown (SB) followed by hard breakdown (HB). The abrupt change of the extracted A and B at the transition region to soft breakdown and to hard breakdown was described by the QPC model [9]. The QPC model includes three different regimes: for SILC, it is represented by (3). For the SB and the HB regime, the tunneling concept is not included, i.e., the $\exp(-Kt_{ox})$ term in (3) is neglected. And for the HB regime, the energy barrier represented by ψ in (3) is different than the barrier in the SB regime. In contrast, Fig. 10 shows different behavior for an irradiated device. The measured log-slope for an irradiated device shows random behavior regardless of subsequent electrical stress until breakdown. Soft breakdown was rarely detected in irradiated devices under postirradiation voltage step-stress.

Fig. 11 summarizes the log-slope of the measured gate leakage current versus applied gate voltage between voltage stress steps for unirradiated and irradiated devices. It is clear that the log-slope of unirradiated devices is increased by electrical stress. In contrast, the log-slope of unirradiated devices is independent of subsequent electrical stress. In addition, Fig. 11 shows that high-LET ion-irradiated devices have larger slopes than fresh devices for moderate stress levels. As defined in the QPC model, the tunneling probability of the traps in dielectric films is related to the cell failure probability. The difference in the log-slope plots for the irradiated and unirradiated devices is due to the existence of latent breakdown paths after high-LET ion stress.

To extract the constants of (5), i.e., ψ and C, we applied a linear regression to measured As and Bs for each device between voltage stress steps before soft or hard breakdown. As shown in Figs. 9 and 10, the irradiated and unirradiated capacitors both exhibit approximately linear relationships between A

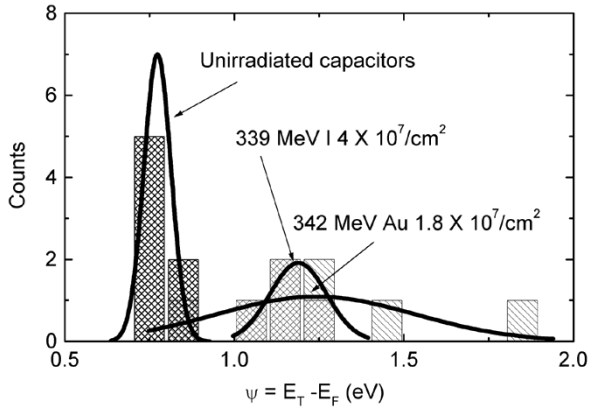

Fig. 12. Histograms of extracted constant ψ of (5) for the capacitors measured for Fig. 11. The mean value of ψ for unirradiated capacitors is 0.8 eV; the mean value of ψ for either 339-MeV I or 342-MeV Au irradiated capacitors is 1.2 eV.

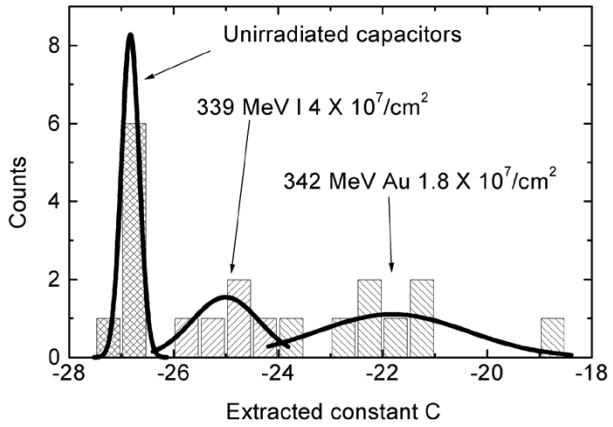

Fig. 13. Histograms of extracted constant C of (5) for the capacitors measured for Fig. 11.

and B. Fig. 12 shows histograms and fitted normal distribution curves of extracted ψ from the capacitors in Fig. 11. The capacitors exposed to Au (LET = 82 MeV/mg/cm^2) and I (LET = 60 MeV/mg/cm^2) both have nearly the same mean value of $\psi = 1.2$ eV, while $\psi = 0.8$ eV for the unirradiated capacitors. In contrast, Fig. 13 shows the extracted value of C from the same data set; all three data sets have different mean values. Even though the fluence for the 342-eV Au (LET = 82 MeV/mg/cm^2) irradiated capacitors is less than half of the 339-eV I (LET = 60 MeV/mg/cm^2) irradiated capacitors, Au irradiated devices have a larger value of C than I irradiated devices. The constant C in (5) implies the number of current paths, i.e., N in (3). Recalling that the physical dimensions and structure of these three sets of capacitors are identical, the difference in C is related to the number of current paths that contribute to the gate leakage current: i.e.,

$$C_1 - C_2 = \ln\left(\frac{N_1}{N_2}\right). \tag{6}$$

Hence, the extracted values of C in Fig. 13 mean that the 342-MeV Au, 1.8×10^7 ions/cm^2, irradiated capacitor has almost 20 times, $\exp(-22 + 25) = 20$, more current paths than the 339-MeV I, 4.0×10^7 ions/cm^2, irradiated capacitor. If most of these current paths in the irradiated capacitors are generated by ion stress, this observation allows us to quantify the difference in defect generation yield for different ions: a 342-MeV Au ion has roughly 44 times larger defect generation yield than a 339-MeV I ion. The defect generation yield increases rapidly with LET, as the comparison of Au (LET = 82) and I (LET = 60) ion irradiation demonstrates; this hypothesis also fits well with the result of Br (LET = 37) ion irradiation, which showed little degradation in Fig. 4.

VI. Conclusion

The experimental data and the model we propose here show that the reliability degradation of a dielectric film due to heavy-ion irradiation is a function of film thickness, incident ion LET, and total fluence. Thinner films are more vulnerable to high-LET heavy ion irradiation than are thicker dielectric films, owing to the greater likelihood that one can induce a completed leakage or breakdown path in a thin oxide than a thick oxide. The defect generation yield is a function of ion LET. Higher-LET ions create more defects than lower-LET ions. The extracted information from the gate-leakage current versus the applied gate voltage supports this assumption. It is clear that these kinds of tests and modeling are useful for providing an increased understanding of dielectric reliability in advanced microelectronic devices with ultrathin gate oxides, which is an area of increasing concern for future space systems. This may also be a significant practical concern in single-event effects testing.

References

[1] F. W. Sexton, D. M. Fleetwood, M. R. Shaneyfelt, P. E. Dodd, and G. L. Hash, "Single event gate rupture in thin gate oxides," *IEEE Trans. Nucl. Sci.*, vol. 44, pp. 2345–2352, Dec. 1997.

[2] L. W. Massengill, B. K. Choi, D. M. Fleetwood, R. D. Schrimpf, K. F. Galloway, M. R. Shaneyfelt, T. L. Meisenheimer, P. E. Dodd, J. R. Schwank, Y. M. Lee, R. S. Johnson, and G. Lucovsky, "Heavy-ion-induced breakdown in ultrathin gate oxides and high-k dielectrics," *IEEE Trans. Nucl. Sci.*, vol. 48, pp. 1904–1912, Dec. 2001.

[3] J. S. Suehle, E. M. Vogel, P. Roitman, J. F. Conley, Jr., A. H. Johnston, B. Wang, J. B. Bernstein, and C. E. Weintraub, "Observation of latent reliability degradation in ultrathin oxides after heavy-ion irradiation," *Appl. Phys. Lett.*, vol. 80, no. 7, pp. 1282–1284, 2002.

[4] B. K. Choi, D. M. Fleetwood, L. W. Massengill, R. D. Schrimpf, K. F. Galloway, M. R. Shaneyfelt, T. L. Meisenheimer, P. E. Dodd, J. R. Schwank, Y. M. Lee, R. S. Johnson, and G. Lucovsky, "Reliability degradation of ultrathin oxynitride and Al_2O_3 gate dielectric films owing to heavy-ion irradiation," *Electron. Lett.*, vol. 38, pp. 157–158, Apr. 2002.

[5] J. Suñé, "New physics-based analytic approach to the thin-oxide breakdown statistics," *IEEE Electron Device Lett.*, vol. 22, pp. 296–298, June 2001.

[6] Y. Wu and G. Lucovsky, "Ultrathin Nitride/Oxide (N/O) gate dielectrics for p^+-polysilicon gated PMOSFETs by combined remote plasma enhanced CVD/thermal oxidation process," *IEEE Electron Device Lett.*, vol. 19, pp. 367–369, Oct. 1998.

[7] F. W. Sexton, D. M. Fleetwood, M. R. Shaneyfelt, P. E. Dodd, G. K. Hash, L. P. Schanwald, R. A. Loemker, K. S. Krisch, M. L. Green, B. E. Weir, and P. J. Silverman, "Precursor ion damage and angular dependence of single event gate rupture in thin oxides," *IEEE Trans. Nucl. Sci.*, vol. 45, pp. 2509–2518, Dec. 1998.

[8] J. H. Stathis, "Percolation models for gate oxide breakdown," *J. Appl. Phys.*, vol. 86, no. 10, pp. 5757–5766, 1999.

[9] E. Miranda and J. Suñé, "Analytical modeling of leakage current through multiple breakdown paths in SiO_2 films," in *Proc. IEEE 39th Annu. Int. Reliability Physics Symp.*, 2001, pp. 367–379.

[10] A. Cester, A. Paccagnella, J. Suñé, and E. Miranda, "Post-radiation-induced soft breakdown conduction properties as a function of temperature," *Appl. Phys. Lett.*, vol. 79, no. 9, pp. 1336–1338, 2001.